A New Multi-objective Comprehensive Optimization Model for Design of Anti-slide Piles

Chao Xu
Institute of Geology and Geophysics Chinese Academy of Sciences
Lei Xue (xuelei@mail.iggcas.ac.cn)
institute Of Geology And Geophysics Chinese Academy Of Sciences https://orcid.org/0000-0002-1408-1126
Yuan Cui
Institute of Geology and Geophysics Chinese Academy of Sciences
Songfeng Guo
Institute of Geology and Geophysics Chinese Academy of Sciences
Mengyang Zhai
Institute of Geology and Geophysics Chinese Academy of Sciences
Fengchang Bu
Institute of Geology and Geophysics Chinese Academy of Sciences
Haoyu Wang
Institute of Geology and Geophysics Chinese Academy of Sciences

Research Article

Keywords: Anti-slide piles, Multi-objective comprehensive optimization model, Optimization index system, Optimization schemes, Numerical simulation, FLAC3D

Posted Date: June 28th, 2021

DOI: https://doi.org/10.21203/rs.3.rs-206508/v1

A New Multi-objective Comprehensive Optimization Model for Design of Anti-slide Piles

Chao Xu[1, 2, 3], Lei Xue[1, 2, 3*], Yuan Cui[1, 2, 3], Songfeng Guo[1, 2, 3], Mengyang Zhai[1, 2, 3], Fengchang Bu[1, 2, 3], Haoyu Wang[1, 2, 3]

***Corresponding author at:**

Key Laboratory of Shale Gas and Geoengineering, Institute of Geology and Geophysics, Chinese Academy of Sciences, Beijing 100029, China.

Tel. /fax: +86 010 82998295.

E-mail address: xuelei@mail.iggcas.ac.cn (Lei Xue).

Email addresses of all co-authors:

xuchao@mail.iggcas.ac.cn (Chao Xu);

xuelei@mail.iggcas.ac.cn (Lei Xue);

cuiyuan@mail.iggcas.ac.cn (Yuan Cui);

guosongfeng@mail.iggcas.ac.cn (Songfeng Guo);

zhaimengyang@mail.iggcas.ac.cn (Mengyang Zhai);

bfc@mail.iggcas.ac.cn (Fengchang Bu)

wanghaoyu2020@mails.ucas.ac.cn (Haoyu Wang)

1. Key Laboratory of Shale Gas and Geoengineering, Institute of Geology and Geophysics, Chinese Academy of Sciences, Beijing, 100029, China

2. Innovation Academy for Earth Science, Chinese Academy of Sciences, Beijing, 100029, China

3. College of Earth and Planetary Sciences, University of Chinese Academy of Sciences, Beijing, 100049, China

Abstract

Landslides have posed a huge threat to the ecological environment and human society all over the world. As the most conventional reinforcement method, anti-slide piles are widely used in the reinforcement of slopes. Currently, more and more attentions have been paid to the low-cost and high-efficiency optimal design of anti-slide piles. However, limitations in the method of the optimization design for slope reinforced with piles still exist. In this paper, a new multi-objective comprehensive optimization method was proposed for the optimization of the slope reinforced with anti-slide piles. The factor of safety, internal force and deflection of piles were selected as the optimization indexes and the optimization index weight was determined by integrating the subjective and objective weight. The influence of the pile location, pile length and pile spacing on the reinforcement effect was analyzed by the numerical simulation. Through the simulation case analysis, the proposed model had achieved good effects on the optimization design of anti-slide piles, which could effectively reduce the engineering costs. The optimization results showed that the best reinforcement effect for the homogeneous slope could be obtained when the anti-slide piles with the critical pile length and small pile spacing was located in the middle of the slope. This provides a new solution for the optimization design of other types of complex slopes, and has broad application prospects.

Keywords Anti-slide piles · Multi-objective comprehensive optimization model · Optimization index system · Optimization schemes · Numerical simulation · FLAC^{3D}

Declarations

Funding

This research was funded by the National Key Research and Development Program of China under Grant Nos. 2018YFC1505302 and 2019YFC1509701, the Strategic Priority Research Program of the Chinese Academy of Sciences under Grant No. XDA23090402, and the National Natural Science Foundation of China under Grant Nos. 41977249 and 42090052.

Conflicts of interest/Competing interests

The authors declare that they have no conflict of interest.

Availability of data and material

Availability. If necessary, please email to the corresponding author.

(Data transparency.)

Code availability

Availability. If necessary, please email to the corresponding author.

(Software application or custom code not applicable.)

Authors' contributions

Conceptualization: Chao Xu, LeiXue; Data curation: Chao Xu, Yuan Cui, Songfeng Guo; Formal analysis: Chao Xu, Lei Xue, Fengchang Bu; Funding acquisition: Lei Xue; Investigation: Chao Xu, Fengchang Bu, Haoyu Wang; Methodology: Chao Xu, LeiXue; Project administration: LeiXue; Resources: LeiXue, Songfeng Guo; Software: Chao Xu, Songfeng Guo; Supervision: LeiXue, Songfeng Guo; Validation: Yuan Cui, Mengyang Zhai, Haoyu Wang; Visualization Chao Xu, Mengyang Zhai; Writing – original draft: Chao Xu; Writing – review & editing: Chao Xu, LeiXue.

1 Introduction

With the rapid development of global engineering construction, slope stability has become a worldwide significant problem in engineering practice (Hassiotis et al. 1997; Li et al. 2020). The anti-slide pile as the most conventional reinforcement method is widely used due to the advantages of strong anti-sliding ability and convenient construction (Cai and Ugai 2000; Kanagasabai et al. 2011; Liu et al. 2020; Wei and Cheng 2009). Therefore, the design of anti-slide pile is crucial. At present, the mainstream design methods for anti-slide pile include loading-structure method (Price and Morgenstern 1967), Viggiani method (Viggiani 1981), Ito Tomio method (Ito and Matsui 1975) and Poulos method (Poulos 1973), which are based on limit equilibrium or displacement compatibility. The basic idea for these methods is to firstly determine the residual pushing force and anti-slide force satisfied with the stability of the slope, then calculate the bending moment and shear force for each pile, and finally give the suitable design parameters such as the pile length, the pile spacing and the pile location (Kanagasabai et al. 2011). However, these methods fail to consider the interaction between pile and soil, which can not accurately reflect the true stability of the slope reinforced with piles.

Recently, more and more scholars (Ausilio et al. 2001; Cai and Ugai 2000; Li et al. 2016; Nian et al. 2008; Won et al. 2005; Yang and Zhang 2020) have realized the fact that the pile length, pile location, pile spacing and other design parameters have a significant impact on the reinforcement of the slope via limit equilibrium methods and finite element methods. For example, the optimization results of pile length show that there is a critical pile length which can achieve the optimal reinforcement effect, and excessive pile length can not increase the factor of safety of the slope but will cause construction waste (Chen et al. 2020; Griffiths et al. 2010; Shooshpasha and Amirdehi 2015; Won et al. 2005). The researches about pile location reveal the fact that the best slope reinforcement effect can be obtained when the anti-slide pile is located in the middle of the slope (Ausilio et al. 2001; Cai and Ugai 2000; Hajiazizi et al. 2017a; Li et al. 2012; Li et al. 2020; Zhang et al. 2017b), Wei and Cheng (2009) even gave the

105 precise pile location which is 0.2m above the middle of the slope. The studies about
106 optimal pile spacing show that the smaller spacing of the anti-slide pile is, the better
107 integrity of reinforced slope is, which is more conducive to the stability of the
108 reinforced slope (Cai and Ugai 2000; Hajiazizi et al. 2017b; Jeong et al. 2003;
109 Kourkoulis et al. 2011; Sun et al. 2016; Zhang et al. 2017a), but the determination of
110 pile spacing mainly depends on the soil arching effect between piles in practical
111 engineering. Although these studies have a guiding significance for the optimization
112 design of anti-slide piles, the optimization results may have some certain deviations
113 which are because the only the factor of safety of reinforced slope is taken as the only
114 optimization objective.

115 In fact, the slope reinforced with piles is a complete organism composed by the slope
116 and anti-slide piles. Numerous cases of the reinforced slope instability (Hu et al. 2020;
117 Li et al. 2010; Li et al. 2013; Liu et al. 2016) show that the optimization design for anti-
118 slide piles need to consider not only the stability of the slope, but also the safety of anti-
119 slide pile itself. Therefore, it is particularly important to consider the internal force and
120 deformation of the pile in the optimization design process. Yang et al. (2011b) and Wang
121 et al. (2015) revealed the internal force and deformation characteristics of pile under
122 various reinforcement schemes, and pointed out that the pile may not be under a safe
123 state when the slope obtained the maximum factor of safety. Zhu et al. (2017) fully
124 considered the change of pile head displacement and established the deformation
125 prediction model for anti-slide piles, which provided theoretical guidance for optimal
126 design. However, their studies failed to consider the coordination and contradiction of
127 various pile elements and give qualitative optimization results. Moreover, the analytic
128 hierarchy process (AHP) (Xu 2013) and multi-objective comprehensive evaluation
129 method (Li and Wei 2018) were used to optimize the design of anti-slide piles based on
130 the evaluation indexes considered the factor of safety and internal force of piles
131 comprehensively, which is concordant with practical situation.

132 In conclusion, it is unreasonable to ignore the safety state of anti-slide piles to
133 evaluate the stability of the slope reinforced. Therefore, in this paper the multi-objective
134 comprehensive optimization model based on improved fuzzy comprehensive

evaluation was developed to optimize the design of anti-slide pile, and the optimization indexes system and the comprehensive index weight was established, the factor of safety, bending moment, shear force and deflection were selected as the optimization indexes. FLAC^{3D} software was used to establish a three-dimensional numerical model which could reflect the interaction between the slope and piles to analyze the changes of factor of safety and the internal force and deformation of anti-slide piles under various reinforcement schemes, and the proposed method was used to optimize. Thus, the proposed optimization model is expected to provide a reference for the optimization design of anti-slide pile engineering.

2 Multi-objective comprehensive optimization model

2.1 Feasibility of the method

Generally, most of the engineering optimization design problems are multi-objective optimization problems and there are usually contradictions between various optimization objectives. Therefore, the results of optimization design based on single factor merely are unreliable. The multi-objective comprehensive optimization model takes the research object as a whole, which has following advantages: 1) it can comprehensively consider the mutual influence between various factors; 2) it can quantify the impact of indexes on optimization goals. In fact, the optimization design of anti-slide piles to strengthen the slope is a multi-objective optimization problem, which could be solved reliably by the multi-objective comprehensive optimization model.

2.2 Optimization design process and method

Figure 1 shows the flowchart of the multi-objective comprehensive optimization model based on an improved fuzzy comprehensive evaluation method.

Fig. 1 Flowchart of the multi-objective comprehensive optimization model.

2.2.1 Determination of the optimal goals

In the design of slope reinforced with anti-slide piles, factors such as pile location,

pile length, and pile spacing are usually considered in order to achieve a good reinforcement effect. However, the overly conservative design has led to high engineering costs in most cases (Hu et al. 2020; Zhao et al. 2006). Therefore, the optimum design of anti-slide piles aims to reduce as many engineering costs as possible while satisfying the safety of supporting structure without affecting the stability of reinforced slope.

2.2.2 Construction of the optimization index system

The stability of slope, the safety of supporting structure and the economy must be taken into account in the selection of evaluating index system, which will determine the accuracy of the optimization model. The index of safety factor reflects the stability of slope reinforced with piles; the indexes of bending moment, internal force and displacement reflect the safety of anti-slide piles. The changes of the above indicators correspond to different optimization schemes (such as different pile locations, pile lengths and pile spacings), and will have an obvious impact on the construction difficulty and engineering cost. Therefore, this paper selects the factor of safety, bending moment, shear force and deflection of anti-slide piles as the main optimization indexes.

2.2.3 Construction of the index function

Supposing that there are n optimization indexes to compose a sample set of optimization indexes $\left\{a_{(i,j)} \mid i=1\sim n, j=1\sim m\right\}$ for all m schemes. In order to make the data highly comparable and the modeling universal, this study adopts the percentage system (Liu et al. 2019) and the maximum-minimum standardization method to standardize the evaluating indexes $a_{(i,j)}$.

The standardized formula for the positive optimization indexes that are positively correlated with the results, such as the factor of safety, can be taken as follows:

$$r_{(i,j)}=\alpha+\beta\cdot e^{\frac{a_{(i,j)}-a_{(i,j)\max}}{a_{(i,j)\max}-a_{(i,j)\min}}} \tag{1}$$

The standardized formula for the negative optimization indexes that are negatively correlated with the results, such as internal force and deflection of piles, can be taken

as follows:

$$r_{(i,j)} = \alpha + \beta \cdot e^{\frac{a_{(i,j)\min} - a_{(i,j)}}{a_{(i,j)\max} - a_{(i,j)\min}}} \tag{2}$$

where $a_{(i,j)\min}$ and $a_{(i,j)\max}$ are the minimum and maximum values of the *i*th index in the *j*th scheme, respectively; $r_{(i,j)}$ is the standardized optimization value, that is, the relative membership value of the *i*th index in the *j*th scheme is subordinate to the optimal value; α and β are constant indicators for constructing the percentile system which meet $\alpha+\beta=100$.

Thus, the fuzzy matrix can be determined as follows:

$$R = \begin{bmatrix} r_{(1,1)} & r_{(1,2)} & \cdots & r_{(1,m)} \\ r_{(2,1)} & r_{(2,2)} & \cdots & r_{(2,m)} \\ \vdots & \vdots & & \vdots \\ r_{(n,1)} & r_{(n,2)} & \cdots & r_{(n,m)} \end{bmatrix}_{n\times m} \tag{3}$$

2.2.4 Determination of index weight

The subjective weight determined by the AHP and objective weight determined by the entropy method are used to establish the comprehensive weight of optimization indexes. Thus, the comprehensive weight of evaluating index can be obtained as follows:

$$w_{(i)} = \frac{w_{s(i)} \cdot w_{o(i)}}{\sum_{i=1}^{n} w_{s(i)} \cdot w_{o(i)}} \tag{4}$$

where $w_{s(i)}$ and $w_{o(i)}$ are the subjective weight and objective weight, respectively. The objective weight $w_{o(i)}$ can be calculated as follows:

$$w_{o(i)} = \frac{1 - e_{(i)}}{\sum_{i=1}^{n} (1 - e_{(i)})} \tag{5}$$

where $e_{(i)}$ is the entropy of the *i*th optimization index.

2.2.5 Analysis and comparison of the optimization results

The fuzzy comprehensive optimization value $k_{(j)}$ can be obtained by synthesizing the weight of each optimization index $w_{(i)}$ and the relative membership value $r_{(i,j)}$ of the

corresponding optimization index in different schemes.

$$k_{(j)} = \sum_{i=1}^{n} \sum_{j=1}^{m} w_{(i)} \cdot r_{(i,j)} \tag{6}$$

The value of $k_{(j)}$ determines the optimal membership degree of different schemes. Generally, the larger the value $k_{(j)}$ is, the more reasonable the scheme is.

3 Determination of optimization indexes and values by numerical simulation

As mentioned above, the factor of safety, internal forces and deflection of the pile are selected as the target value for the optimization design of anti-slide piles, which will be significantly affected by the reinforcement options such as pile lengths, pile location and pile spacing (Cai and Ugai 2000). Therefore, the acquisition of optimization values is the key premise of comprehensive optimization. For this reason, numerical simulation method is selected to obtain the accurate optimization index value and verify the reliability of the proposed model.

3.1 Establishment of numerical model

The homogeneous slope models of different reinforcement schemes with anti-slide piles have been established by the finite difference software FLAC^{3D} as shown in Fig. 2, and the reinforced slope model considered by many researchers (Cai and Ugai 2000; Wei and Cheng 2009; Won et al. 2005) is adopted excepts some changes in the dimensions and gradients of slope. The uniform boundary conditions follow: the displacement of bottom boundary is completely fixed, the horizontal displacement of left and right boundary is restrained, and the upper boundary is free to move. Mohr-Coulomb constitutive model is selected to simulate the deformation and failure behavior of slope soil. The initial stress field only considers the self-weight stress field. The entirely run-through of plastic zone is regarded as the criterion of slope instability. Details about the parameters of soil are shown in Table 1. The factor of safety is calculated via the strength reduction method (SRM) (Griffiths and Lane 1999; Matsui and San 1992; Wei et al. 2009; Zheng and Zhao 2004; Zienkiewicz et al. 1975).

Fig. 2 Numerical model of slope reinforced with anti-slide piles. L_x, L_p, L and S stand for the distance from the pile to the slope toe, the horizontal length of the slope, the pile length and the pile spacing, respectively. For interpretation of the references to color in this figure, the reader is referred to the electronic version of this page.

Fig. 3 Mechanical model of pile (modified after Wang et al. (2015)). Spring A, spring B stand for the normal coupling spring and the shear coupling spring, respectively. For interpretation of the references to color in this figure, the reader is referred to the electronic version of this page.

Table 1 Physical and mechanical parameters of the slope

Considering that the internal force of any section can not be obtained directly with the solid element piles, and the accuracy of the calculating results is affected by the mesh size (Chen et al. 2019), the structural element pile was used to simulate the anti-slide pile due to the advantages of easy modeling, high calculation efficiency and guaranteed accuracy (Griffiths et al. 2010; Lee et al. 2014). The mechanical model of pile structural element is shown in Fig. 3, the transfer of force and bending moment between the pile element and the mesh element could be realized by the normal coupling spring (Spring A) and the shear coupling spring (Spring B) at the position of structural element node, which realizes the coupling effect between pile and soil. Details about the parameters of anti-slide piles are shown in Table 2.

Table 2 Physical and mechanical parameters of anti-slide piles

3.2 Influence of anti-slide pile location on slope reinforcement

The influence of the anti-slide pile reinforcement location on the optimization indexes is studied with the pile spacing of 5m. The pile location is defined by the ratio of pile horizontal distance from the slope toe (L_x) to the horizontal length of the slope (L_p), which is shown in Fig. 2. The effects of various pile locations and pile lengths on the factor of safety of the slope reinforced with piles are shown in Fig. 4, and the

maximum factor of safety for each pile location is shown in Fig. 5. It can be obtained from the Figs. 4 and 5 that the factor of safety is the largest and the reinforcement effect is the best when the anti-slide pile is located in the middle of the slope (L_x/L_p=0.5); on the contrary, the factor of safety is the smallest and the reinforcement effect is poor when the pile location is at the toe of the slope (L_x/L_p=0.1). The results obtained in present research are similar to those of Cai and Ugai (2000), Griffiths et al. (2010) and Yang et al. (2011b).

Fig. 4 Factors of safety for various pile lengths and pile locations. For interpretation of the references to color in this figure, the reader is referred to the electronic version of this page.

Fig. 5 Maximum factor of safety for various pile locations

The distribution of shear strain increment zone is consistent with the large deformation area of the slope, which can reflect the position of the critical slip surface precisely (Zheng 2012). The effect of various pile locations on the maximum shear strain increment and the position of critical slip surface obtained by FISH language is shown in Figs. 6 and 7, respectively. It is seen from Figs. 6 and 7 that the change of pile location has a significant impact on the distribution of critical slip surface. In other word, the concentration region of shear strain increment and the run-through critical slip surface tends to form behind the anti-slide piles gradually when the pile location is located at the lower-middle part of the slope (L_x/L_p=0.1, 0.3), however, the concentration region of shear strain increment and the run-through critical slip surface tends to form in front of the anti-slide piles eventually when the pile location is located at the upper-middle part of the slope (L_x/L_p=0.7, 0.9). Therefore, it is concluded that there are three different failure modes of slope reinforced with piles. These failure modes are as follows: (1) slide will originate from posterior surface of the piles when the pile location is located in the lower-middle part; (2) the critical slip surface is divided into two disconnected parts and slide is not easy to originate when the pile location is locked in the middle part; (3) slide will originate from anterior of the piles

when the pile location is located in the upper-middle part.

Fig. 6 Contour of maximum shear strain increment for various pile locations. **a** without piles; **b** L_x/L_p=0.1, pile length L=12m; **c** L_x/L_p=0.3, pile length L=18m; **d** L_x/L_p=0.5, pile length L=28m; **e** L_x/L_p=0.7, pile length L=30m; **f** L_x/L_p=0.9, pile length L=24m. (Taking the pile spacing of S=5m as an example). For interpretation of the references to color in this figure, the reader is referred to the electronic version of this page.

Fig. 7 The critical slip surface for various pile lengths and pile locations. **a** L_x/L_p=0.1; **b** L_x/L_p=0.3; **c** L_x/L_p=0.5; **d** L_x/L_p=0.7; **e** L_x/L_p=0.9. (Taking the pile spacing of S=5m as an example). For interpretation of the references to color in this figure, the reader is referred to the electronic version of this page.

The effect of various pile locations on anti-slide pile behaviors is shown in Fig. 8. The bending moment, the shear force and the deflection of the pile increase at first and then decrease with the pile location from the toe upwards the top of slope, and the maximum points of both pile behaviors appear in the pile located at the middle part of the slope. It should be noted that the depth of maximum bending moment or the shear force valued zero at each pile location has a good correspondence with the position of critical slip surface. Thus, the various pile locations not only affect the factor of safety of the slope reinforced, but also change the distribution of the inter force of pile.

Fig. 8 Anti-slide pile behaviors for various pile locations. **a** Bending moment; **b** Shear force; **c** Deflection. For interpretation of the references to color in this figure, the reader is referred to the electronic version of this page.

3.3 Influence of anti-slide pile length on slope reinforcement

The determination of pile length is the key to the optimization design of anti-slide piles. Too short pile length is not conducive to the slope stability (Kourkoulis et al. 2011), and too long pile length will increase the engineering costs (Yang et al. 2011b).

Figure 4 shows the effect of the pile length on the factor of safety of the slope reinforced with anti-slide piles. Taking the pile location of L_x/L_p=0.3 as an example, as expected, the factor of safety of reinforced slope increase with the increasing of the pile length. However, when the pile length exceeds a certain length (18m in present study) which is named the critical pile length (Griffiths et al. 2010), the factor of safety is close to a constant gradually, and this is because the enough anti-sliding force can be provided by the embedded length of pile in stable stratum to resist the sliding force.

In order to further study the effect of various pile lengths on the slope reinforcement, the maximum shear strain increment and the critical slip surface are obtained at the pile location of L_x/L_p=0.3, as shown in Figs. 9 and 7b. It can be observed that with the increase of pile length, the zone of maximum shear strain increment is gradually divided into two parts which are not disconnected, but when the pile length exceeds 18m, the run-through zone of maximum shear strain increment is reformed (Fig. 9e). As shown in Fig. 7b, the critical slip surface becomes deeper with the increase of pile length, and the failure mode of reinforced slope changes from shallow sliding to deep sliding. This is mainly due to the complex structure formed by pile-soil interaction improves the strength of soil around the pile. However, when the pile length is more than 18m, the critical slip surface suddenly becomes shallow and passes through the top of pile. The main reason for this is that deep sliding needs more energy due to the reinforcement of anti-slide piles, while the shallow sliding only requires less energy to produce.

Fig. 9 Contour of maximum shear strain increment for various pile lengths. **a** Pile length L=6m; **b** Pile length L=10m; **c** Pile length L=14m; **d** Pile length L=16m; **e** Pile length L=18m; **f** Pile length L=22m (Taking the pile location of L_x/L_p=0.3 and the pile spacing of S=5m as an example). For interpretation of the references to color in this figure, the reader is referred to the electronic version of this page.

The effect of various pile lengths on the pile behaviors is shown in Fig. 10. It can be seen that, when the pile length is less than the critical pile length (18m), the bending moment (Fig. 10a) increases with the increase of the pile length, and the position of the

maximum bending moment is continuously away from the top of piles, which corresponds well to the position of the critical slip surface (Fig. 7b); the positive shear force of piles (Fig. 10b) increases as the pile length increases; the pile deflection increases with the increase of the pile length, but it should be noted that the distribution of deflection is almost linearly (Fig. 10c) when the pile length is short, which indicates that the pile is prone to overturning failure under too short pile length. When the pile length exceeds the critical pile length, the bending moment, shear force and deflection all tend to be a stable distribution, which is consistent with the change law of the factor of safety.

Fig. 10 Anti-slide pile behaviors for various pile lengths. **a** Bending moment; **b** Shear force; **c** Deflection. For interpretation of the references to color in this figure, the reader is referred to the electronic version of this page.

3.4 Influence of anti-slide pile spacing on slope reinforcement

Taking the pile location of L_x/L_p=0.3 and the critical pile length (18m) as an example, the effect of various pile spacings on reinforced slope is studied. Figure 11 shows the change of factors of safety under various pile spacings, it can be seen that the factor of safety of the reinforced slope decreases with the increase of pile spacing.

Fig. 11 Factors of safety for various pile spacings under the critical pile length. *Fos*, *S* stand for the factor of safety and the pile spacing, respective. For interpretation of the references to color in this figure, the reader is referred to the electronic version of this page.

The effects of various pile spacings on the maximum shear strain increment and the critical slip surface is shown in Fig. 12. It can be seen that when the pile spacing is small, the critical slip surface between two anti-slide piles is shallow and almost passes over the top of the pile. With the increasing of the pile spacing, the critical slip surface gradually becomes deeper and the instability mode has changed. When the pile spacing is large enough (Fig. 12a4), a complete and run-through critical slip surface is formed

392 gradually, which is nearly close to the critical slip surface of slope unreinforced (Fig.
393 6a). This may be related to the evolution of soil arch under various pile spacings.
394
395 **Fig. 12** Contour of shear strain increment and the critical slip surface for various pile spacings under
396 the critical pile length. **a1, b1** Pile spacing S=4m; **a2, b2** Pile spacing S=5m; **a3, b3** Pile spacing
397 S=6m; **a4, b4** Pile spacing S=7m (Taking the pile location of L_x/L_p=0.3 and the critical pile length
398 (L=18m) as an example). For interpretation of the references to color in this figure, the reader is
399 referred to the electronic version of this page.
400
401 The effect of various pile spacings on the pile behaviors is shown in Fig. 13. It can
402 be concluded that the bending moment (Fig. 13a) and the shear force (Fig. 13b) increase
403 with the increase of pile spacing. This can be explained by the fact that the anti-slide
404 piles act as the retaining walls and the integrity and strength of the pile and soil are
405 improved significantly while the pile spacing decreases, so that soil wouldn't reach the
406 limit state until the soil with large deformation (Cai and Ugai 2000), which can be
407 demonstrated by the pile deflection (Fig. 13c); soil arch between piles disappears
408 gradually when the pile spacing increases and only a single anti-slide pile works at this
409 moment.
410
411 **Fig. 13** Pile behaviors for various pile spacings under the critical pile length. **a** Bending moment;
412 **b** Shear force; **c** Deflection. For interpretation of the references to color in this figure, the reader is
413 referred to the electronic version of this page.
414
415 To sum up, the interaction between pile and soil is fully considered with the
416 numerical simulation method and the factor of safety, internal force and deformation of
417 piles obtained under various reinforcement options are more realistic, which is in good
418 agreement with previous studies (Cai and Ugai 2000; Gao et al. 2015; Hajiazizi et al.
419 2017b; Jeong et al. 2003; Sun et al. 2016; Yang et al. 2011b). Therefore, it is feasible to
420 obtain the optimization indexes values by the numerical simulation and to optimize
421 designs combined with the proposed multi-objective comprehensive optimization

422 model.

423 4 Results and discussion

424 The factor of safety and the bending moment, shear force and deflection of piles were
425 obtained based on the numerical simulation under various reinforcement schemes, and
426 results were analyzed with the proposed multi-objective comprehensive optimization
427 model.

428 4.1 Results analysis

429 4.1.1 Calculation results of indicator value and weight

430 The indicator value of optimization system was determined by the numerical
431 simulation. It should be noted that the factor of safety of reinforced slope belongs to the
432 positive optimization index and the bending moment, shear force and deflection belong
433 to the negative optimization indexes, so Eqs. (1) and (2) were used for normalization
434 calculation, respectively. The calculation results of indicator value under different
435 reinforcement schemes are shown in Tables 3-7.

436

437 **Table 3** The standardized values of optimization indexes (Pile location L_x/L_p=0.1)

438

439 **Table 4** The standardized values of optimization indexes (Pile location L_x/L_p=0.3)

440

441 **Table 5** The standardized values of optimization indexes (Pile location L_x/L_p=0.5)

442

443 **Table 6** The standardized values of optimization indexes (Pile location L_x/L_p=0.7)

444

445 **Table 7** The standardized values of optimization indexes (Pile location L_x/L_p=0.9)

446

447 Decision-making AHP method was adopted to determine the subjective weight of
448 optimization indexes. Considering intentions of decision makers, engineering
449 experience and judgements of geological hazard experts, 1-9 ratio scaling method was
450 taken to define the relative importance and subjective weight of each optimization index,
451 as shown in Table 8. According to the principle of AHP (Brunelli 2015), the maximum

eigenvalue of judgment matrix (λ_{max}) is 4.25, the consistency index (CI) is 0.08, the consistency ratio (CR) equals 0.09 and is less than 0.1, which meets the consistency requirements.

Table 8 Subjective weight determination for optimization indexes

The objective weight was calculated by Eq. (5) based on the entropy method, and the results are shown in Table 9.

The comprehensive weight of each evaluating index was calculated via Eq. (4) as shown in Table 9. Among them, the weight of factor of safety is the largest and that of shear force of pile is the smallest.

Table 9 Comprehensive weight determination for optimization indexes

4.1.2 Optimal results analysis

The fuzzy comprehensive optimization value $k_{(j)}$ was calculated according to Eq. (6) (where α=60 and β=40). The comprehensive optimization results is shown in Fig. 14. It can be seen that the results under various reinforcement schemes are significantly different. According to the principle of optimal judgement, the comprehensive optimization value corresponding to scheme 35 is the highest, that is, the anti-slide pile located in the middle of slope, with the pile length of 28m and pile location of 4m is the most reasonable choice. In addition, more details could be drawn as follows:

Fig.14 Optimization results based on the multi-objective comprehensive optimization model. *S*, L_x/L_p stand for the pile spacing and the pile location, respectively. For interpretation of the references to color in this figure, the reader is referred to the electronic version of this page.

(1) When the anti-slide pile is located in the middle or upper-middle part (L_x/L_p=0.7) of the slope, the effect of slope reinforced with piles is obviously better than that of the toe or shoulder of the slope, which is in good agreement with the numerical simulation

(Section 3.2) and results obtained by Hassiotis et al. (1997) and Yang et al. (2011a).

(2) The increase of pile length can significantly improve the reinforcement effect of the slope, but it does not mean that the longer the pile length, the better the reinforcement effect. For example, when the pile is located in the lower-middle part (L_x/L_p=0.3) with the pile spacing of 5m, the value of $k_{(j)}$ increases slightly or even decreases when the pile length exceeds 18m (Fig. 14), this is mainly because excessive pile length leads to the increase of internal force of anti-slide piles under the premise of meeting design requirements of factor of safety, which is not conductive to the safety of piles.

(3) The smaller pile spacing is, the better reinforcement effect is. In addition, the reinforcement effect of piles located in the location of L_x/L_p=0.7 with pile spacing of 5m is significantly better than that in the location of L_x/L_p=0.5 with pile spacing of 6m, therefore, the pile spacing can be appropriately reduced to improve the reinforcement effect in actual engineering when the anti-pile is located in non-middle position.

4.2 Discussion

4.2.1 Comparisons with results under various α and β values

In order to make the evaluating indexes more comparable and keep as much information as possible about the changes in the optimization index values, the constants α and β were introduced to construct the normalization functions (Eqs. (1) and (2)) based on the percentage system. Figure 15 presents the effect of various combinations of α and β on the optimization results of anti-slide piles. The result indicates that curves of the optimization result under various values of α and β present the approximately parallel relationship and have exactly the same changing law. Besides, the larger the value of α is, the greater the optimization value for the corresponding scheme. However, the changes of α and β only change the absolute value of optimization results and amplitude of variation of curves, but have no effects on the final optimization results.

Fig.15 Comparison of optimization results with different α and β values (Refer to Tables 3-7 or Fig. 14 for detailed reinforcement scheme corresponding to scheme number). For interpretation of the

512 references to color in this figure, the reader is referred to the electronic version of this page.

513

514 4.2.2 Comparisons with results under various weights

515 The final optimization results under various index weight types are shown in Fig. 16.
516 It can be seen that, the result (Red line in Fig. 16) by using the subjective weight only
517 indicates that scheme 35 is the optimal reinforcement option, which is basically
518 consistent with the conclusion drawn via the proposed method in this article, but the
519 optimization values of each scheme have little difference, which is easy to make wrong
520 decisions due to the human factors implications and inaccurate data. The optimization
521 result (Blue line in Fig. 16) obtained only by the objective weight reveals that the
522 reinforcement effect is the worst when the anti-slide pile is located in the middle part
523 of the slope, which is totally at variance with the practical engineering experience, this
524 may be the reason that the index weight of entropy method is determined according to
525 the variation degree of the index, which ignores the importance of the index itself.
526 Comparison of the three different optimization results shows that the comprehensive
527 weight proposed in this article make the optimization results more scientific and
528 reasonable. Therefore, with the continuous development of habitable earth construction,
529 the proposed multi-objective comprehensive optimization model will play an important
530 role in the design of slopes reinforcement.

531

532 **Fig.16** Comparison of optimization results with different weights (Refer to Tables 3-7 or Fig. 14 for
533 detailed reinforcement scheme corresponding to scheme number). For interpretation of the
534 references to color in this figure, the reader is referred to the electronic version of this page.

535

536 4.2.3 Limitation of the proposed method

537 In the current study, the numerical simulation method was used to obtain the values
538 of evaluating indexes in the multi-objective comprehensive optimization model.
539 Although more reasonable optimization results had been achieved, more engineering
540 cases and field monitoring data are still needed to further study to verify the accuracy
541 and applicability of this proposed model. Besides, the comprehensive weight used in

this article considers the advantages of both subjective and objective weight, and minimizes the adverse effects of shortcomings of two on optimization results, but it is still unavoidable that the weight obtained goes against the actual situation, which leads to make an absurd decision-making. Therefore, it is necessary to further optimize the index weight based on methods of big data, machine learning and deep learning.

5 Conclusion

The multi-objective comprehensive optimization model for the design of slope reinforced with anti-slide piles was proposed based on the traditional fuzzy comprehensive evaluation method, and the reliability of the model was verified by finite element numerical simulation. The main conclusions are as follows:

(1) According to the numerical simulation results, various pile locations, pile lengths and pile spacings have significant effects on the slope reinforced. The best reinforcement effect could be obtained when the pile is located in the middle part of the slope. The increase of the pile length can increase the reinforcement effect obviously, but it will not continue to increase the slope stability when the pile length exceeds the critical pile length. The larger the pile spacing is, the worse the stability of the slope and safety of the anti-slide pile are.

(2) The factor of safety, internal force and deflection of the anti-slide pile were selected as the optimization index system to ensure that the optimized reinforcement scheme could meet the stability of the pile-slope system. Meanwhile, the comprehensive weight was determined combined with the subjective and objective, which is more in line with practical engineering cases.

(3) Based on the three-dimensional slope numerical model, the proposed multi-objective comprehensive optimization model was applied to optimize various reinforcement schemes, which obtained reasonable optimization results. This provides a new solution for the optimization design of other types of complex slopes, and has broad application prospects.

Acknowledgements This research was funded by the National Key Research and Development Program of China under Grant Nos. 2018YFC1505302 and 2019YFC1509701, the Strategic Priority Research Program of the Chinese Academy of Sciences under Grant No. XDA23090402, and the National Natural Science Foundation of China under Grant Nos. 41977249 and 42090052.

Compliance with ethical standards

Conflict of interest The authors declare that they have no conflict of interest.

References

Ausilio E, Conte E, Dente G (2001) Stability analysis of slopes reinforced with piles. COMPUT GEOTECH 28(08):591-611. https://doi.org/10.1016/S0266-352X(01)00013-1

Brunelli M (2015) Introduction to the analytic hierarchy process. Springer International Publishing. https://doi.org/10.1007/978-3-319-12502-2

Cai F, Ugai K (2000) Numerical analysis of the stability of a slope reinforced with piles. SOILS FOUND 40:73-84. https://doi.org/10.3208/sandf.40.73

Chen C, Wang W, Lv HY (2019) Stability analysis of slope reinforced with composite anti-slide pile model. ROCK SOIL MECH 40(08):3207-3217. https://doi.org/10.16285/j.rsm.2018.0747

Chen FY, Zhang RH, Wang Y, Liu H, Böhlke T, Zhang WG (2020) Probabilistic stability analyses of slope reinforced with piles in spatially variable soils. INT J APPROX REASON 122:66-79. https://doi.org/10.1016/j.ijar.2020.04.006

Gao YF, Ye M, Zhang F (2015) Three-dimensional analysis of slopes reinforced with piles. J CENT SOUTH UNIV 22(06):2322-2327. https://doi.org/10.1007/s11771-015-2757-6

Griffiths D, Lin H, Cao P (2010) A comparison of numerical algorithms in the analysis of pile reinforced slopes. 175-183. https://doi.org/10.1061/41095(365)14

Griffiths DV, Lane PA (1999) Slope stability analysis by finite elements. GEOTECHNIQUE 49(03):387-403. https://doi.org/10.1680/geot.1999.49.3.387

Hajiazizi M, Bavali M, Fakhimi A (2017a) Numerical and experimental study of the optimal location of concrete piles in a saturated sandy slope. INT J CIV ENG 16(10):1293-1301. https://doi.org/10.1007/s40999-017-0155-1

Hajiazizi M, Mazaheri A, Orense R (2017b) Analytical approach to evaluate stability of pile-stabilized slope. SCI IRAN 25(5):2525-2536. https://doi.org/10.24200/sci.2017.4218

Hassiotis S, Chameau JL, Gunaratne M (1997) Design method for stabilization of slopes with piles. J GEOTECH GEOENVIRON 123(04):314-323. https://doi.org/10.1061/(ASCE)1090-0241(1997)123:4(314)

Hu F, Chao W, Feng L (2020) Research on failure mode of slope reinforced by single micro-pixe based on ultimate resistance. HIGHWAY 65(04):12-18.

Ito T, Matsui T (1975) Methods to estimate lateral force acting on stabilizing piles. SOILS FOUND 15(04):43-59. https://doi.org/10.3208/sandf1972.15.4_43

Jeong S, Kim B, Won J, Lee J (2003) Uncoupled analysis of stabilizing piles in weathered slopes. COMPUT GEOTECH 30(08):671-682. https://doi.org/10.1016/j.compgeo.2003.07.002

Kanagasabai S, Smethurst J, Powrie W (2011) Three-dimensional numerical modelling of discrete piles used to stabilize landslides. CAN GEOTECH J 48(09):1393-1411. https://doi.org/10.1139/t11-046

Kourkoulis R, Gelagoti F, Anastasopoulos I (2011) Slope stabilizing piles and pile-Groups: parametric study and design insights. J GEOTECH GEOENVIRON 137(07):663-677. https://doi.org/10.1061/(ASCE)GT.1943-5606.0000479

Lee FH, Goh SH, Banerjee S (2014) Earthquake-induced bending moment in fixed-head piles in soft clay. GEOTECHNIQUE 64(06):431-446. https://doi.org/10.1680/geot.12.P.195

Li CD, Chen WQ, Song YJ, Gong WP, Zhao QH (2020) Optimal Location of Piles in Stabilizing Slopes Based on a Simplified Double-Row Piles Model. KSCE J CIV ENG 24(02):377-389. https://doi.org/10.1007/s12205-020-0712-z

Li CD, Tang HM, Hu XL, Wang LQ (2013) Numerical modelling study of the load sharing law of anti-sliding piles based on the soil arching effect for Erliban landslide, China. KSCE J CIV ENG 17(06):1251-1262. https://doi.org/10.1007/s12205-013-0074-x

Li QL, Wei HW (2018) Optimization design of pile location on slope based on multi-objective comprehensive evaluation method. J RAILW SCIENCE ENG 15(06):1445-1452. https://doi.org/10.19713/j.cnki.43-1423/u.2018.06.011

Li RJ, Zheng W, Shao SJ, Liu K (2010) Analysis of local sliding mechanism of Longdong slope reinforced with stabilizing piles. ROCK SOIL MECH 31(S2):322-327. https://doi.org/10.16285/j.rsm.2010.s2.032

Li XP, Pei XJ, Gutierrez M, He SM (2012) Optimal location of piles in slope stabilization by limit analysis. ACTA GEOTECH 7(03):253-259. https://doi.org/10.1007/s11440-012-0170-y

Li XP, Su LJ, He SM, Xu J (2016) Limit equilibrium analysis of seismic stability of slopes reinforced with a row of piles. INT J NUMER ANAL MET 40(08):1241-1250. https://doi.org/10.1002/nag.2484

Liu B, Su PD, Qiu P, Li ZB (2016) Numerical simulation of the anti-slide pile overtopping of high slope. J ENG GEOL 24(s1):940-946. https://doi.org/10.13544/j.cnki.jeg.2016.s1.136

Liu B, Zhang FL, Wan WY, Luo XW (2019) Multi-objective decision-making for the ecological operation of built reservoirs based on the improved comprehensive fuzzy evaluation method. WATER RESOUR MANAG 33(11):3949-3964. https://doi.org/10.1007/s11269-019-02349-x

Liu XY, Cai GJ, Liu LL, Zhou ZJ (2020) Investigation of internal force of anti-slide pile on landslides considering the actual distribution of soil resistance acting on anti-slide piles. NAT HAZARDS 102(03):1369-1392. https://doi.org/10.1007/s11069-020-03971-4

Matsui T, San K-C (1992) Finite element slope stability analysis by shear strength reduction technique. SOILS FOUND 32:59-70. https://doi.org/10.3208/sandf1972.32.59

Nian TK, Chen GQ, Luan MT, Yang Q, Zheng DF (2008) Limit analysis of the stability of slopes reinforced with piles against landslide in nonhomogeneous and anisotropic soils. CAN GEOTECH J 45(08):1092-1103. https://doi.org/10.1139/t08-042

Poulos H (1973) Analysis of piles in soil undergoing lateral movement. ASCE J Soil Mech Found Div 99(05):391-406.

Price VE, Morgenstern NR (1967) The analysis of stability of general slip surface. GEOTECHNIQUE 15(03):393-394. https://10.1680/geot.1968.18.3.393

Shooshpasha I, Amirdehi HA (2015) Evaluating the stability of slope reinforced with one row of free head piles. ARAB J GEOSCI 8(04):2131-2141. https://doi.org/10.1007/s12517-014-1272-7

Sun SW, Zhao F, Zhang K (2016) Stability of Slopes Reinforced with Truncated Piles. ADV MATER SCI ENG 2016:1-16. https://doi.org/10.1155/2016/1570983

Viggiani C (1981) Ultimate lateral load on piles used to stabilize landslides. INT J ROCK MECH MIN 21(03):555-560. https://doi.org/10.1016/0148-9062(84)91821-7

Wang CC, Li JT, Liao J, Hao RQ, Liu B (2015) Stability analysis of slope reinforced with piles and optimization. J CENT SOUTH UNIV 46(01):231-237. https://doi.org/10.11817/j.issn.1672-7207.2015.01.031

Wei WB, Cheng YM (2009) Strength reduction analysis for slope reinforced with one row of piles. COMPUT GEOTECH 36(07):1176-1185. https://doi.org/10.1016/j.compgeo.2009.05.004

Wei WB, Cheng YM, Li L (2009) Three-dimensional slope failure analysis by the strength reduction and limit equilibrium methods. COMPUT GEOTECH 36(1-2):70-80.

https://doi.org/10.1016/j.compgeo.2008.03.003

Won J, You K, Jeong S, Kim S (2005) Coupled effects in stability analysis of pile–slope systems. COMPUT GEOTECH 32(04):304-315. https://doi.org/10.1016/j.compgeo.2005.02.006

Xu JC (2013) Analytic hierarchy process for assessing factors influencing the stability of soil slopes reinforced with piles. ENVIRON EARTH SCI 70(04):1507-1514. https://doi.org/10.1007/s12665-013-2236-z

Yang GH, Zhang YX, Zhang YC, Tang JM (2011a) Optimal site of anti-landslide piles based on deformation field of slopes. CHIN J GEOTECH ENG 33(S1):8-13.

Yang SK, Ren XH, Zhang JX (2011b) Study on embedded length of piles for slope reinforced with one row of piles. J ROCK MECH GEOTECH 3(02):167-178. https://doi.org/10.3724/SP.J.1235.2011.00167

Yang XL, Zhang S (2020) Stability analysis of 3D cracked slope reinforced with piles. COMPUT GEOTECH 122:103544. https://doi.org/10.1016/j.compgeo.2020.103544

Zhang G, Wang LP, Wang YL (2017a) Pile reinforcement mechanism of soil slopes. ACTA GEOTECH 12(05):1035-1046. https://doi.org/10.1007/s11440-017-0543-3

Zhang J, Wang H, Huang HW, Chen LH (2017b) System reliability analysis of soil slopes stabilized with piles. ENG GEOL 229:45-52. https://doi.org/10.1016/j.enggeo.2017.09.009

Zhao WB, Luo WQ, Feng Y (2006) Study on designing system of anti-slide piles based on reliability theory. ROCK SOIL MECH 27(S2):952-957.

Zheng YR (2012) Development and application of numerical limit analysis for geological materials. CHIN J ROCK MECH ENG 31(07):1297-1316. https://doi.org/10.3969/j.issn.1000-6915.2012.07.001

Zheng YR, Zhao SY (2004) Application of strength reduction fem in soil and rock slope. CHIN J ROCK MECH ENG 23(19):3381-3388.

Zhu Y, Zhu HH, Zhang W, Shi B (2017) Parametric analysis on factors influencing stability of slopes reinforced by anti-slide piles. J ENG GEOL 25(03):833-840. https://doi.org/10.13544/j.cnki.jeg.2017.03.031

Zienkiewicz OC, Humpheson C, Lewis RW (1975) Associated and non-associated visco-plasticity and plasticity in soil mechanics. GEOTECHNIQUE 25(04):671-689. https://doi.org/10.1680/geot.1975.25.4.671

Table captions

706 # Table list

707 **Table 1** Physical and mechanical parameters of the slope

Material	Young modulus E (MPa)	Poisson ratio v	Unit weight γ（kN/m^3）	Cohesion c (kPa)	Friction angle φ（°）
Soil	200	0.25	20	24	24

708

709 **Table 2** Physical and mechanical parameters of anti-slide piles

Parameter	Value	Parameter	Value	Parameter	Value
Young modulus (GPa)	30	Coupling-cohesion-shear (MPa)	19	Coupling-cohesion-normal (MPa)	19
Poisson ratio	0.21	Coupling-stiffness-shear (MN/m^2)	100	Coupling-stiffness-normal (MN/m^2)	100
Moi-z (m^4)	2.0	Coupling-friction-shear (°)	22	Coupling-friction-normal (°)	22
Moi-y (m^4)	4.5	Density (kg/m^3)	2500	Coupling-gap- normal	on
Moi-polar (m^4)	6.5	Cross-sectional-area (m^2)	6.0	Perimeter (m)	10

710

711 **Table 3** The standardized values of optimization indexes (Pile location L_x/L_p=0.1)

Schemes			Optimization indexes							
Scheme number	Pile length (m)	Pile spacing (m)	Factor of safety	Standardized value	Bending moment (MN·m)	Standardized value	Shear force (MN)	Standardized value	Deflection (mm)	Standardized value
1	4		1.086	74.7152	0.0095	100.0000	0.0074	100.0000	4.8118	99.4518
2	6		1.117	75.7793	0.0417	99.6925	0.0226	98.5427	8.4043	98.4878
3	8	4	1.117	75.7793	0.0442	99.6688	0.0213	98.6627	3.9533	99.6857
4	10		1.117	75.7793	0.0532	99.5826	0.0223	98.5667	3.1692	99.9005
5	12		1.117	75.7793	0.0608	99.5106	0.0226	98.5423	2.8076	100.0000
6	4		1.102	75.2551	0.0175	99.9236	0.0129	99.4631	6.5990	98.9692
7	6		1.117	75.7793	0.0543	99.5728	0.0288	97.9629	6.6706	98.9500
8	8	5	1.117	75.7793	0.0609	99.5098	0.0293	97.9093	4.9446	99.4157
9	10		1.117	75.7793	0.0638	99.4828	0.0271	98.1150	3.3483	99.8513
10	12		1.117	75.7793	0.0721	99.4038	0.0272	98.1127	2.8712	99.9825
11	4		1.09	74.8483	0.0138	99.9584	0.0103	99.7188	6.5623	98.9791
12	6		1.113	75.6378	0.0595	99.5228	0.0321	97.6549	11.8975	97.5731
13	8	6	1.113	75.6378	0.0615	99.5043	0.0300	97.8458	4.6817	99.4871
14	10		1.113	75.6378	0.0816	99.3142	0.0344	97.4396	3.9269	99.6929
15	12		1.113	75.6378	0.0922	99.2144	0.0389	97.0341	3.8866	99.7039

712

713 **Table 4** The standardized values of optimization indexes (Pile location L_x/L_p=0.3)

Schemes			Optimization indexes							
Scheme number	Pile length (m)	Pile spacing (m)	Factor of safety	Standardized value	Bending moment (MN·m)	Standardized value	Shear force (MN)	Standardized value	Deflection (mm)	Standardized value
16	12		1.160	77.3839	0.1821	98.3779	0.0504	96.0076	14.2851	96.9604
17	16		1.215	79.6764	0.6264	94.4982	0.1123	90.9501	33.3707	92.4087
18	18	4	1.270	82.2712	0.7789	93.2585	0.1303	89.6197	26.1902	94.0514
19	20		1.300	83.8280	0.8090	93.0197	0.1325	89.4608	17.0491	96.2636
20	24		1.300	83.8280	0.8404	92.7722	0.1313	89.5469	11.6363	97.6407
21	12		1.133	76.3583	0.1649	98.5366	0.0498	96.0617	9.6011	98.1719
22	16		1.246	81.0993	0.6604	94.2182	0.1265	89.8973	12.2886	97.4720
23	18	5	1.289	83.2449	0.9646	91.8099	0.1619	87.4226	14.0635	97.0168
24	20		1.293	83.4553	1.0041	91.5100	0.1640	87.2829	14.2040	96.9810
25	24		1.300	83.8280	1.4549	88.2801	0.1645	87.2477	15.8044	96.5757
26	12		1.160	77.3839	0.3075	97.2409	0.0766	93.7729	31.0931	92.9209
27	16		1.230	80.3525	0.7946	93.1336	0.1570	87.7515	24.2187	94.5168
28	18	6	1.258	81.6773	0.9650	91.8071	0.1699	86.8879	25.4380	94.2282
29	20		1.258	81.6773	0.9748	91.7318	0.1704	86.8555	17.2764	96.2069
30	24		1.258	81.6773	1.0455	91.1986	0.1645	87.2477	14.4811	96.9105

714

715 **Table 5** The standardized values of optimization indexes (Pile location L_x/L_p=0.5)

Schemes			Optimization indexes							
Scheme number	Pile length (m)	Pile spacing (m)	Factor of safety	Standardized value	Bending moment (MN·m)	Standardized value	Shear force (MN)	Standardized value	Deflection (mm)	Standardized value
31	16		1.180	78.1849	0.2541	97.7203	0.0602	95.1560	25.6001	94.1900
32	20		1.300	83.8280	0.8677	92.5579	0.1292	89.7043	62.4966	86.5192
33	24	4	1.418	91.0819	1.8774	85.5549	0.2116	84.2840	106.3539	79.6067
34	26		1.418	91.0819	1.8824	85.5242	0.2127	84.2177	61.3435	86.7306
35	28		1.530	100.0000	2.8983	80.0042	0.2743	80.8337	123.5003	77.4232
36	16		1.145	76.8064	0.3022	97.2879	0.0721	94.1499	28.0213	93.6247
37	20		1.293	83.4553	1.1134	90.6947	0.1666	87.1045	76.4857	84.0838
38	24	5	1.395	89.5128	2.1853	83.7351	0.2588	81.6380	100.0991	80.4696
39	26		1.478	95.5792	2.2550	83.3420	0.2587	81.6456	66.7549	85.7528
40	28		1.508	98.0663	3.8532	75.9089	0.3673	76.6011	84.9950	82.7132
41	16		1.176	78.0218	0.3864	96.5426	0.0874	92.8965	37.9742	91.3974
42	20		1.285	83.0364	1.3168	89.2330	0.1927	85.4354	90.5684	81.8580
43	24	6	1.400	89.8471	2.4538	82.2550	0.2895	80.0747	103.3196	80.0207
44	26		1.387	88.9858	2.7704	80.6271	0.3193	78.6676	78.3015	83.7846
45	28		1.473	95.1808	4.1784	74.7152	0.4166	74.7152	145.3559	74.9888

716

717 **Table 6** The standardized values of optimization indexes (Pile location L_x/L_p=0.7)

Schemes			Optimization indexes							
Scheme number	Pile length (m)	Pile spacing (m)	Factor of safety	Standardized value	Bending moment (MN·m)	Standardized value	Shear force (MN)	Standardized value	Deflection (mm)	Standardized value
46	20		1.211	79.4999	0.3937	96.4782	0.0732	94.0553	32.0181	92.7119
47	24		1.336	85.8405	1.0760	90.9715	0.1330	89.4261	75.6355	84.2252
48	28	4	1.457	93.9356	2.0822	84.3294	0.1997	84.9990	125.5488	77.1791
49	30		1.480	95.7399	2.6618	81.1717	0.2387	82.7269	122.7642	77.5117
50	32		1.488	96.3897	2.9517	79.7496	0.2556	81.8113	103.0020	80.0645
51	20		1.200	79.0228	0.4453	96.0301	0.0832	93.2364	33.7602	92.3218
52	24		1.324	85.1514	1.3312	89.1322	0.1662	87.1340	82.7357	83.0693
53	28	5	1.430	91.9335	2.4631	82.2050	0.2432	82.4798	118.0213	78.0931
54	30		1.470	94.9439	3.3541	77.9320	0.3105	79.0716	137.2803	75.8460
55	32		1.465	94.5526	3.2635	78.3262	0.2992	79.6064	99.8248	80.5083
56	20		1.227	80.2154	0.7506	93.4853	0.1230	90.1551	76.1495	84.1396
57	24		1.309	84.3159	1.5558	87.6040	0.1944	85.3250	86.4370	82.4888
58	28	6	1.395	89.5128	2.8636	80.1714	0.3007	79.5317	113.0908	78.7179
59	30		1.434	92.2224	3.9434	75.5683	0.3672	76.6034	148.0320	74.7152
60	32		1.434	92.2224	4.0986	74.9994	0.3759	76.2567	119.7689	77.8767

718

719 **Table 7** The standardized values of optimization indexes (Pile location L_x/L_p=0.9)

Schemes			Optimization indexes							
Scheme number	Pile length (m)	Pile spacing (m)	Factor of safety	Standardized value	Bending moment (MN·m)	Standardized value	Shear force (MN)	Standardized value	Deflection (mm)	Standardized value
61	20		1.184	78.3495	0.2075	98.1443	0.0426	96.7041	26.5008	93.9786
62	22		1.223	80.0341	0.3840	96.5639	0.0594	95.2280	37.1647	91.5729
63	26	4	1.254	81.4829	0.9130	92.2062	0.0995	91.9336	34.1422	92.2369
64	28		1.258	81.6773	1.1250	90.6095	0.1173	90.5810	31.4219	92.8465
65	30		1.262	81.8735	1.2151	89.9549	0.1244	90.0488	28.7058	93.4666
66	20		1.176	78.0218	0.2396	97.8525	0.0490	96.1354	26.2770	94.0310
67	22		1.227	80.2154	0.5513	95.1253	0.0776	93.6928	51.5052	88.6042
68	26	5	1.238	80.7225	1.1881	90.1491	0.1294	89.6878	42.1948	90.4981
69	28		1.246	81.0993	1.3405	89.0674	0.1421	88.7823	35.4616	91.9454
70	30		1.246	81.0993	1.4169	88.5392	0.1472	88.4215	31.7616	92.7697
71	20		1.195	78.8097	0.4345	96.1232	0.0721	94.1487	67.1803	85.6775
72	22		1.211	79.4999	0.6530	94.2790	0.0918	92.5473	53.6024	88.1941
73	26	6	1.230	80.3525	1.3353	89.1033	0.1513	88.1436	44.3365	90.0516
74	28		1.238	80.7225	1.6504	86.9846	0.1803	86.2146	44.0597	90.1089
75	30		1.238	80.7225	1.4539	88.2873	0.1574	87.7222	30.4846	93.0592

720

721 **Table 8** Subjective weight determination for optimization indexes

Optimization indexes	Factor of safety	Bending moment	Shear force	Deflection	Subjective weight
Factor of safety	1	3	7	6	0.5570
Bending moment	1/3	1	5	4	0.2693
Shear force	1/7	1/5	1	1/4	0.0532
Deflection	1/6	1/4	4	1	0.1205

722

723 **Table 9** Comprehensive weight determination for optimization indexes

Optimization indexes	Subjective weight	Objective weight	Comprehensive weight
Factor of safety	0.5570	0.3984	0.7216
Bending moment	0.2693	0.1485	0.1301
Shear force	0.0532	0.1334	0.0231
Deflection	0.1205	0.3197	0.1252

724

Figure captions

Fig. 1 Flowchart of the multi-objective comprehensive optimization model.

Fig. 2 Numerical model of slope reinforced with anti-slide piles. L_x, L_p, L and S stand for the distance from the pile to the slope toe, the horizontal length of the slope, the pile length and the pile spacing, respectively. For interpretation of the references to color in this figure, the reader is referred to the electronic version of this page.

Fig. 3 Mechanical model of pile (modified after Wang et al. (2015)). Spring A, spring B stand for the normal coupling spring and the shear coupling spring, respectively. For interpretation of the references to color in this figure, the reader is referred to the electronic version of this page.

Fig. 4 Factors of safety for various pile lengths and pile locations. For interpretation of the references to color in this figure, the reader is referred to the electronic version of this page.

Fig. 5 Maximum factor of safety for various pile locations

Fig. 6 Contour of maximum shear strain increment for various pile locations. **a** without piles; **b** L_x/L_p=0.1, pile length L=12m; **c** L_x/L_p=0.3, pile length L=18m; **d** L_x/L_p=0.5, pile length L=28m; **e** L_x/L_p=0.7, pile length L=30m; **f** L_x/L_p=0.9, pile length L=24m. (Taking the pile spacing of S=5m as an example). For interpretation of the references to color in this figure, the reader is referred to the electronic version of this page.

Fig. 7 The critical slip surface for various pile lengths and pile locations. **a** L_x/L_p=0.1; **b** L_x/L_p=0.3; **c** L_x/L_p=0.5; **d** L_x/L_p=0.7; **e** L_x/L_p=0.9. (Taking the pile spacing of S=5m as an example). For interpretation of the references to color in this figure, the reader is referred to the electronic version of this page.

Fig. 8 Anti-slide pile behaviors for various pile locations. **a** Bending moment; **b** Shear force; **c** Deflection. For interpretation of the references to color in this figure, the reader is referred to the electronic version of this page.

Fig. 9 Contour of maximum shear strain increment for various pile lengths. **a** Pile length L=6m; **b** Pile length L=10m; **c** Pile length L=14m; **d** Pile length L=16m; **e** Pile length L=18m; **f** Pile length L=22m (Taking the pile location of L_x/L_p=0.3 and the pile spacing of S=5m as an example). For interpretation of the references to color in this figure, the reader is referred to the electronic version of this page.

Fig. 10 Anti-slide pile behaviors for various pile lengths. **a** Bending moment; **b** Shear force; **c** Deflection. For interpretation of the references to color in this figure, the reader is referred to the electronic version of this page.

Fig. 11 Factors of safety for various pile spacings under the critical pile length. *Fos*, *S* stand for the factor of safety and the pile spacing, respective. For interpretation of the references to color in this figure, the reader is referred to the electronic version of this page.

Fig. 12 Contour of shear strain increment and the critical slip surface for various pile spacings under the critical pile length. **a1, b1** Pile spacing S=4m; **a2, b2** Pile spacing S=5m; **a3, b3** Pile spacing S=6m; **a4, b4** Pile spacing S=7m (Taking the pile location of L_x/L_p=0.3 and the critical pile length (L=18m) as an example). For interpretation of the references to color in this figure, the reader is referred to the electronic version of this page.

Fig. 13 Pile behaviors for various pile spacings under the critical pile length. **a** Bending moment; **b** Shear force; **c** Deflection. For interpretation of the references to color in this figure, the reader is referred to the electronic version of this page.

Fig.14 Optimization results based on the multi-objective comprehensive optimization model. S, L_x/L_p stand for the pile spacing and the pile location, respectively. For interpretation of the references to color in this figure, the reader is referred to the electronic version of this page.

Fig.15 Comparison of optimization results with different α and β values (Refer to Tables 3-7 or Fig. 14 for detailed reinforcement scheme corresponding to scheme number). For interpretation of the references to color in this figure, the reader is referred to the electronic version of this page.

Fig.16 Comparison of optimization results with different weights (Refer to Tables 3-7 or Fig. 14 for detailed reinforcement scheme corresponding to scheme number). For interpretation of the references to color in this figure, the reader is referred to the electronic version of this page.

Figure list

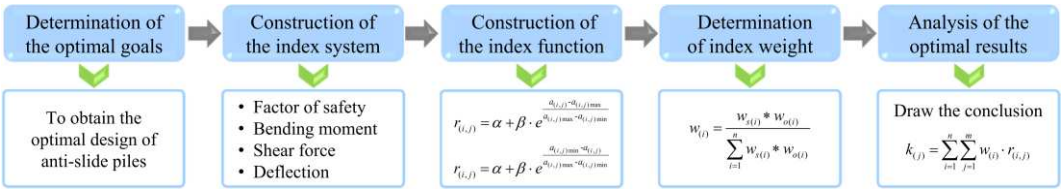

Fig.1 Flowchart of the multi-objective comprehensive optimization model.

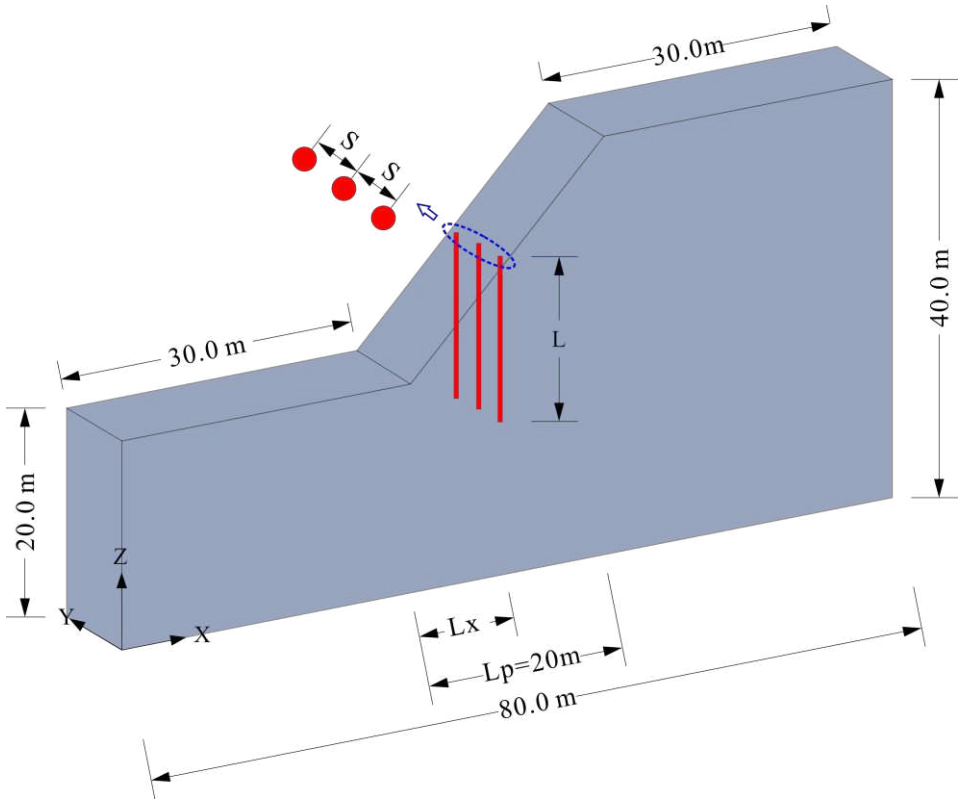

Fig. 2 Numerical model of slope reinforced with anti-slide piles. L_x, L_p, L and S stand for the distance from the pile to the slope toe, the horizontal length of the slope, the pile length and the pile spacing, respectively. For interpretation of the references to color in this figure, the reader is referred to the electronic version of this page.

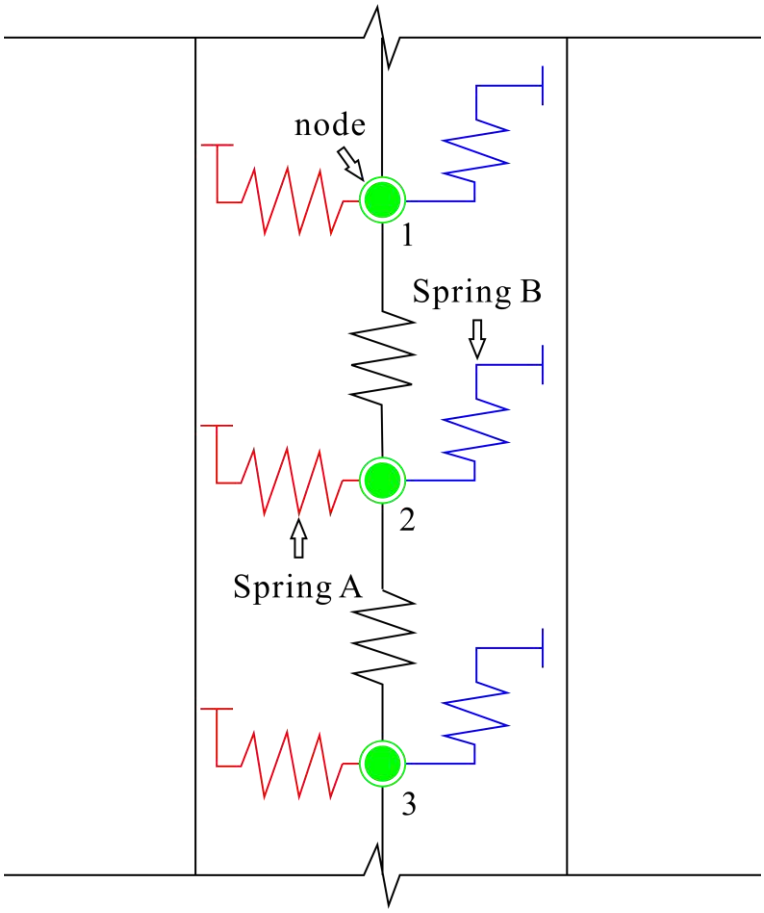

788

789

790 **Fig. 3** Mechanical model of pile (modified after Wang et al. (2015)). Spring A, spring B stand for
791 the normal coupling spring and the shear coupling spring, respectively. For interpretation of the
792 references to color in this figure, the reader is referred to the electronic version of this page.

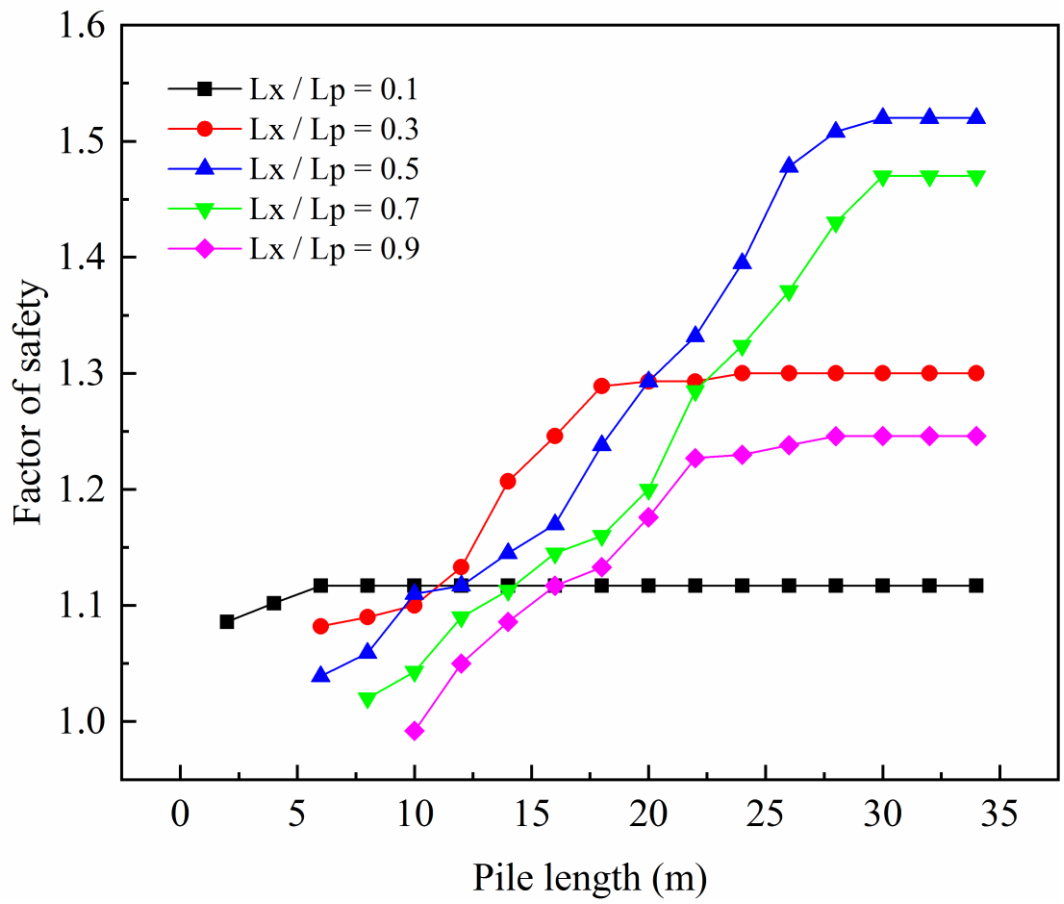

793

794

795 **Fig. 4** Factors of safety for various pile lengths and pile locations. For interpretation of the references

796 to color in this figure, the reader is referred to the electronic version of this page.

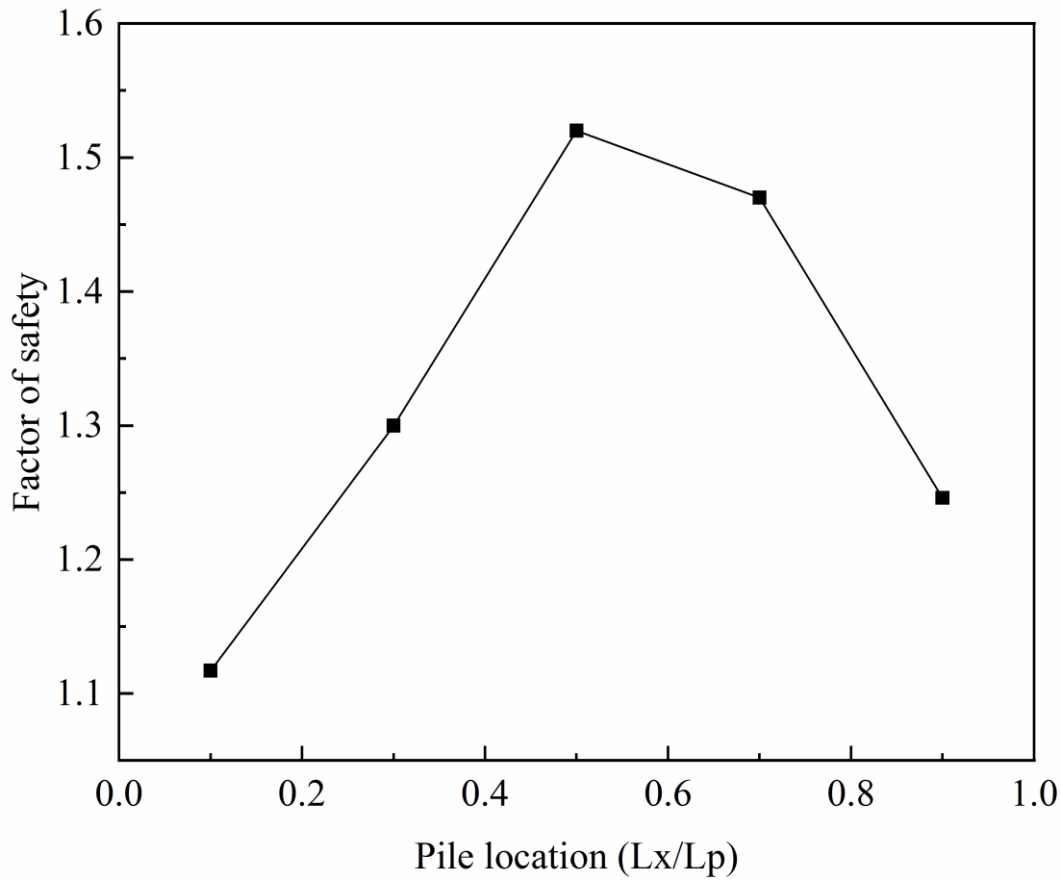

797

798

799 **Fig. 5** Maximum factor of safety for various pile locations

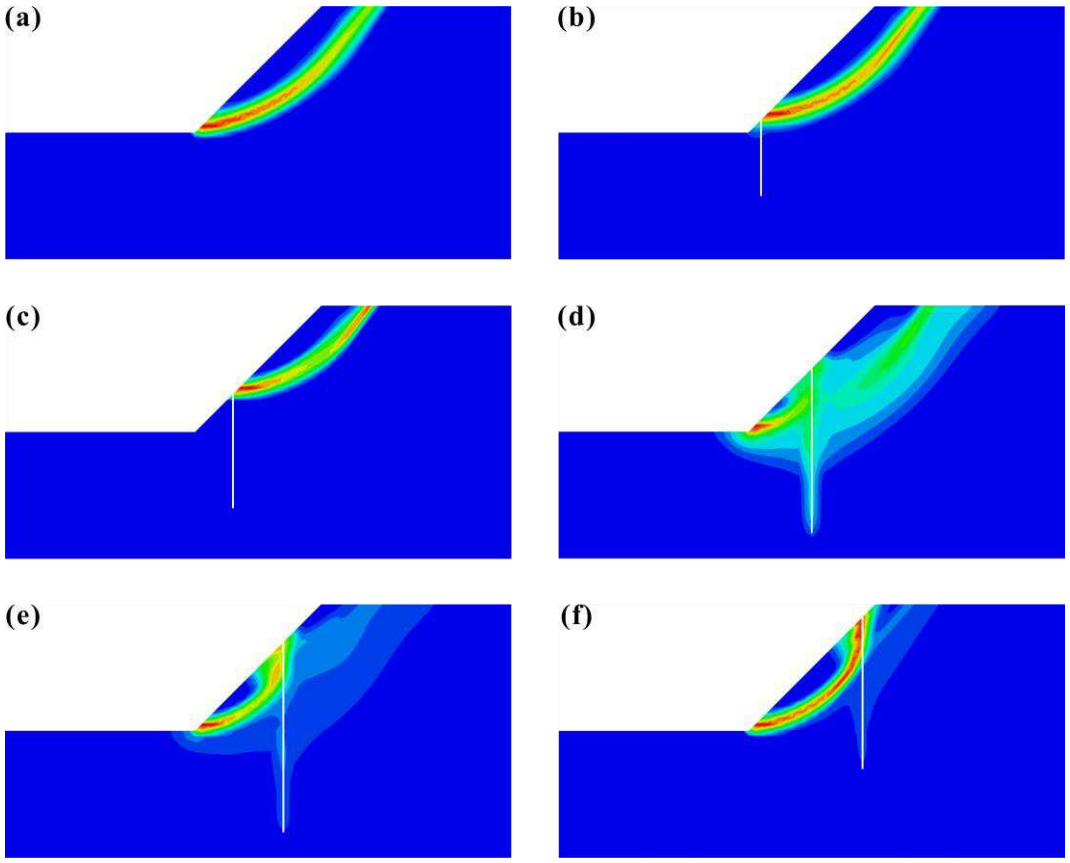

Fig. 6 Contour of maximum shear strain increment for various pile locations. **a** without piles; **b** L_x/L_p=0.1, pile length L=12m; **c** L_x/L_p=0.3, pile length L=18m; **d** L_x/L_p=0.5, pile length L=28m; **e** L_x/L_p=0.7, pile length L=30m; **f** L_x/L_p=0.9, pile length L=24m. (Taking the pile spacing of S=5m as an example). For interpretation of the references to color in this figure, the reader is referred to the electronic version of this page.

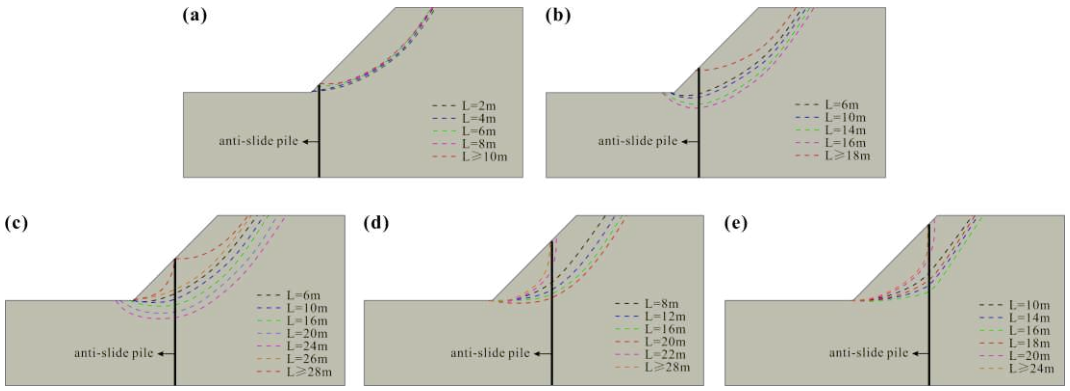

807

808

809 **Fig. 7** The critical slip surface for various pile lengths and pile locations. **a** L_x/L_p=0.1; **b** L_x/L_p=0.3;
810 **c** L_x/L_p=0.5; **d** L_x/L_p=0.7; **e** L_x/L_p=0.9. (Taking the pile spacing of S=5m as an example). For
811 interpretation of the references to color in this figure, the reader is referred to the electronic version
812 of this page.

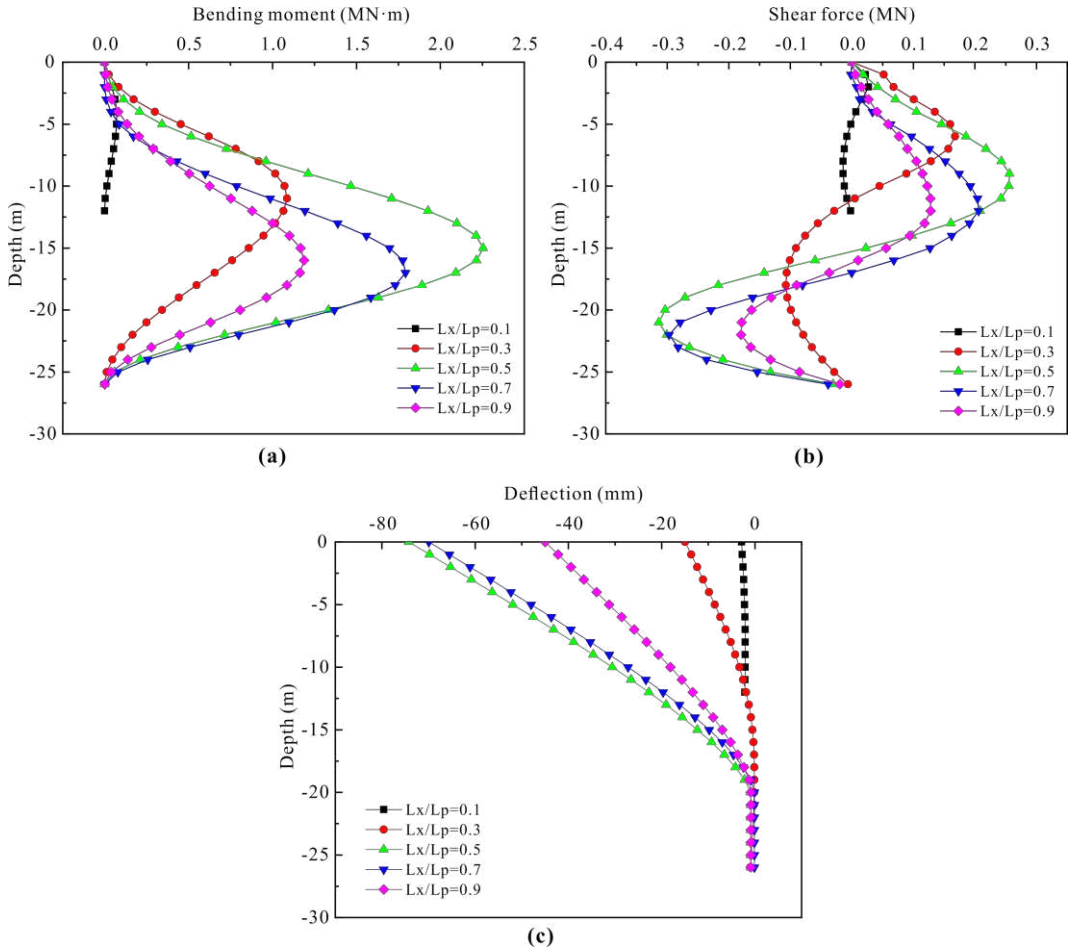

Fig. 8 Anti-slide pile behaviors for various pile locations. **a** Bending moment; **b** Shear force; **c** Deflection. For interpretation of the references to color in this figure, the reader is referred to the electronic version of this page.

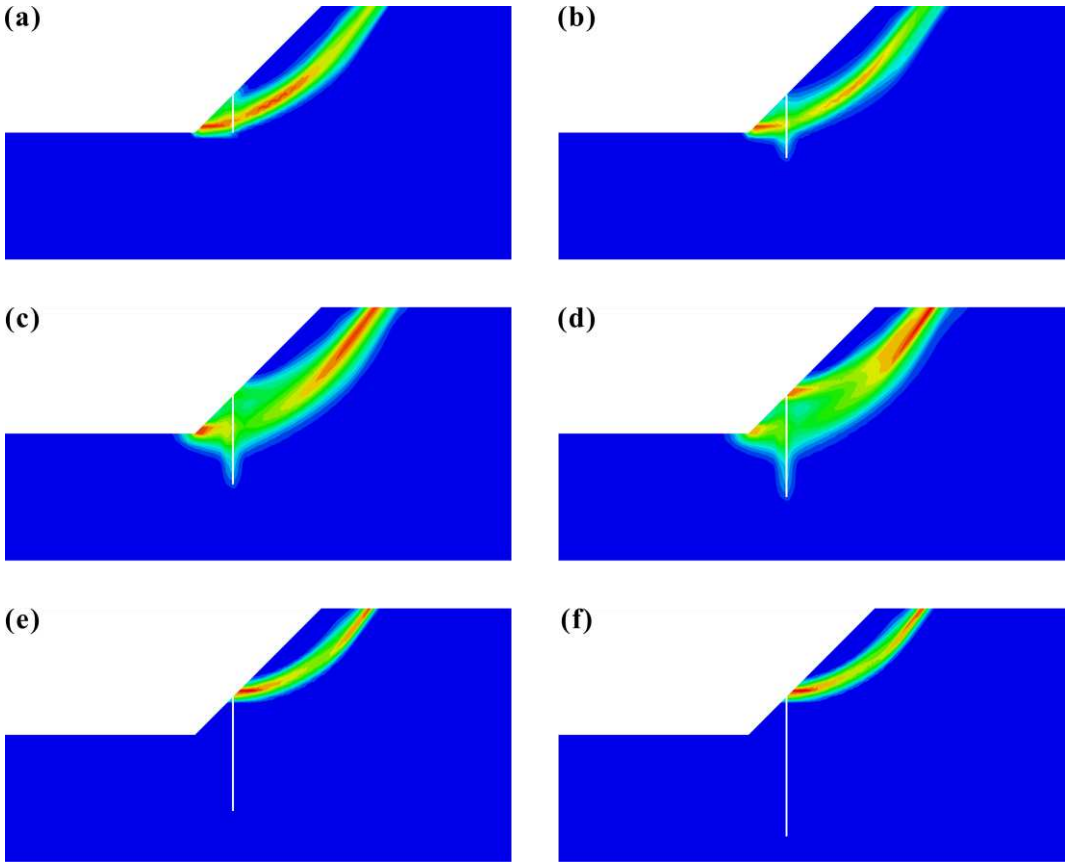

Fig. 9 Contour of maximum shear strain increment for various pile lengths. **a** Pile length L=6m; **b** Pile length L=10m; **c** Pile length L=14m; **d** Pile length L=16m; **e** Pile length L=18m; **f** Pile length L=22m (Taking the pile location of L_x/L_p=0.3 and the pile spacing of S=5m as an example). For interpretation of the references to color in this figure, the reader is referred to the electronic version of this page.

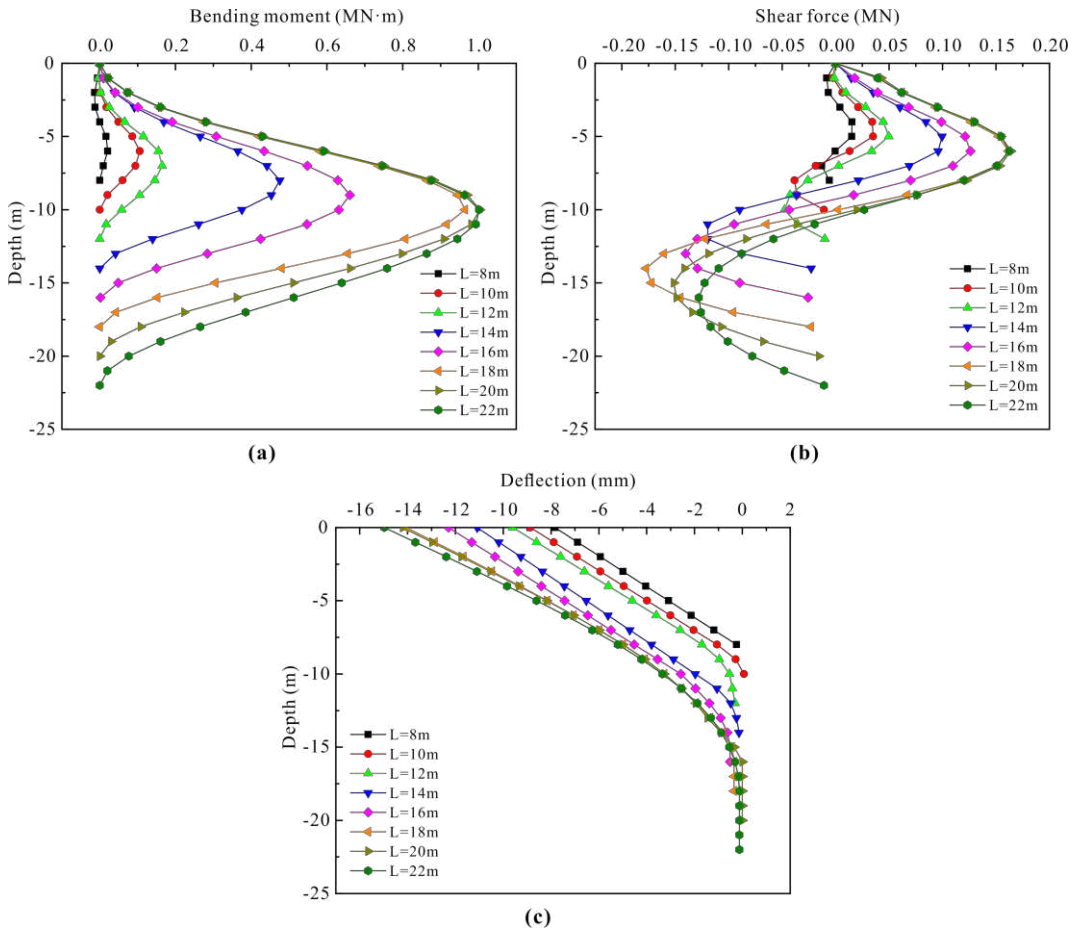

825

826

827 **Fig. 10** Anti-slide pile behaviors for various pile lengths. **a** Bending moment; **b** Shear force; **c**
828 Deflection. For interpretation of the references to color in this figure, the reader is referred to the
829 electronic version of this page.

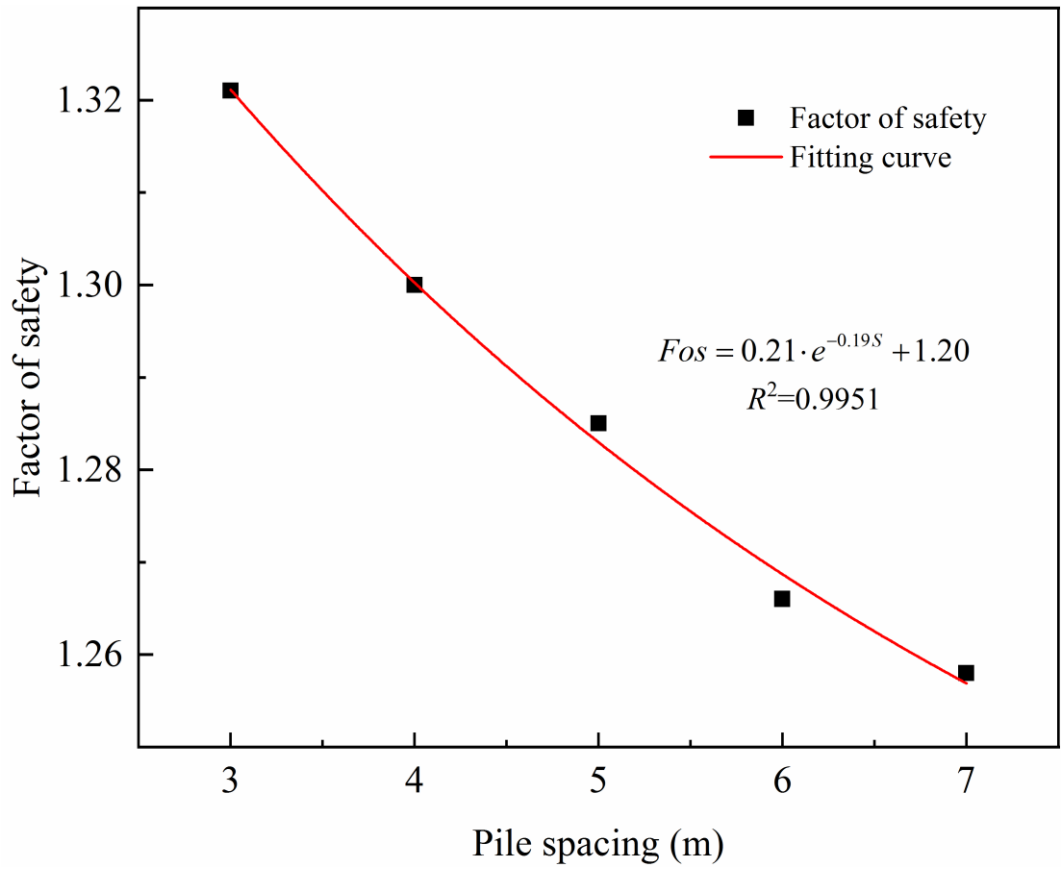

Fig. 11 Factors of safety for various pile spacings under the critical pile length. *Fos*, *S* stand for the factor of safety and the pile spacing, respective. For interpretation of the references to color in this figure, the reader is referred to the electronic version of this page.

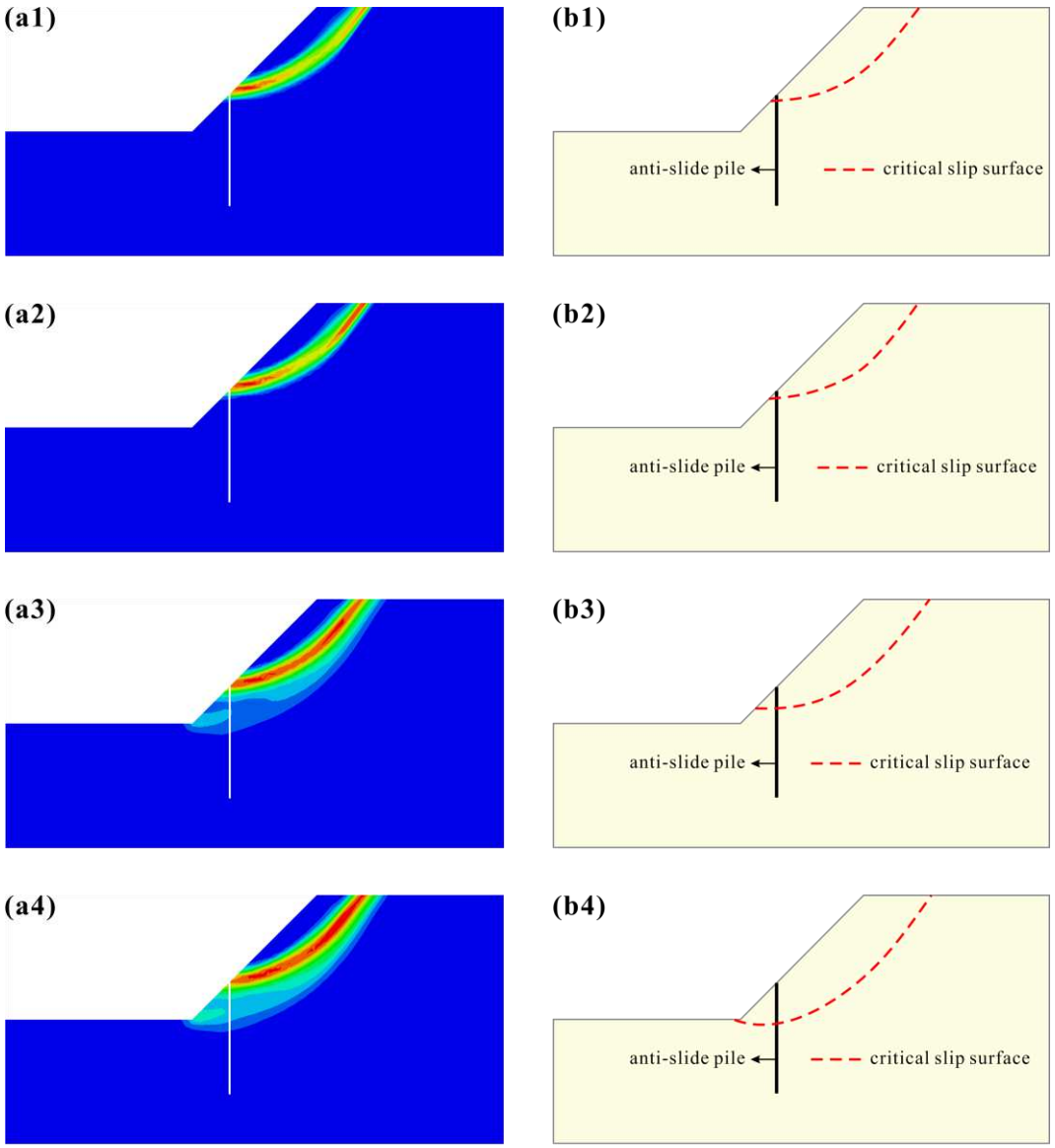

(a) Contour of shear strain increment (b) The critical slip surface

Fig. 12 Contour of shear strain increment and the critical slip surface for various pile spacings under the critical pile length. **a1, b1** Pile spacing S=4m; **a2, b2** Pile spacing S=5m; **a3, b3** Pile spacing S=6m; **a4, b4** Pile spacing S=7m (Taking the pile location of L_x/L_p=0.3 and the critical pile length (L=18m) as an example). For interpretation of the references to color in this figure, the reader is referred to the electronic version of this page.

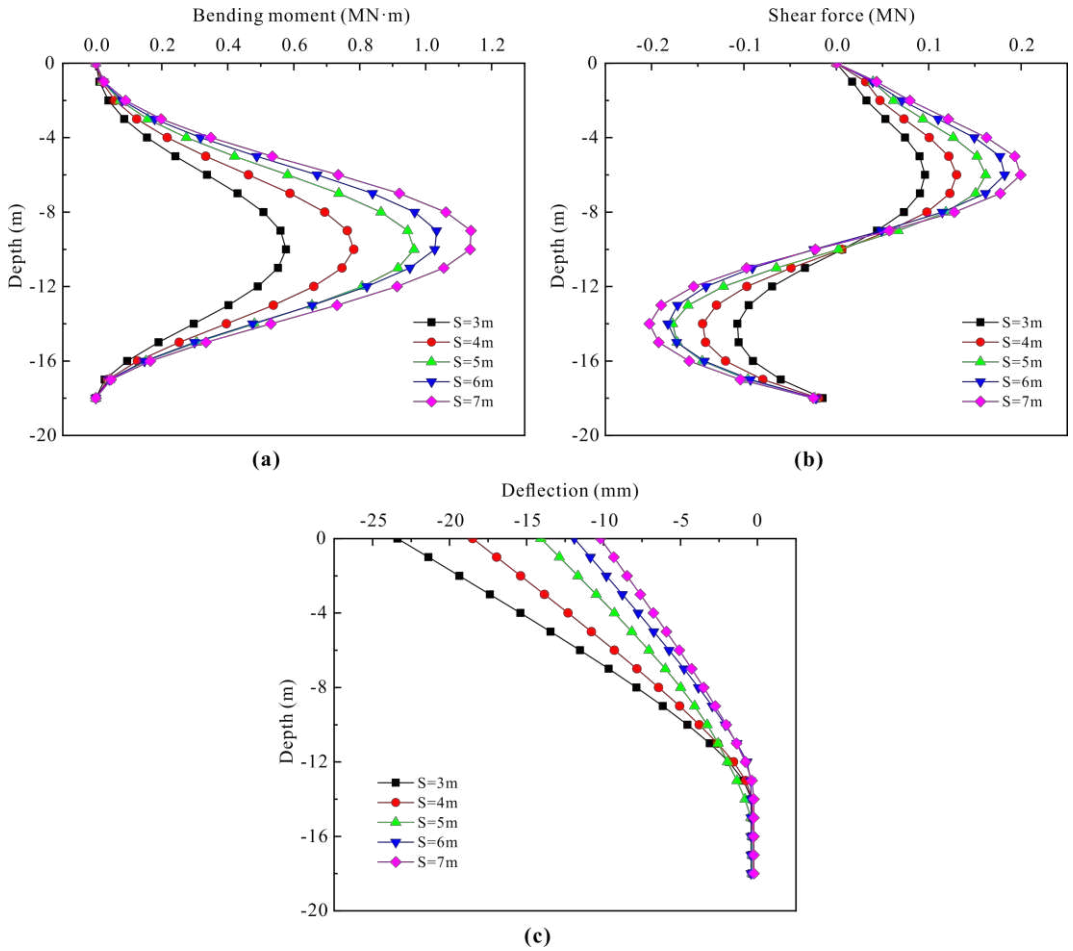

842

843

844 **Fig. 13** Pile behaviors for various pile spacings under the critical pile length. **a** Bending moment;

845 **b** Shear force; **c** Deflection. For interpretation of the references to color in this figure, the reader is

846 referred to the electronic version of this page.

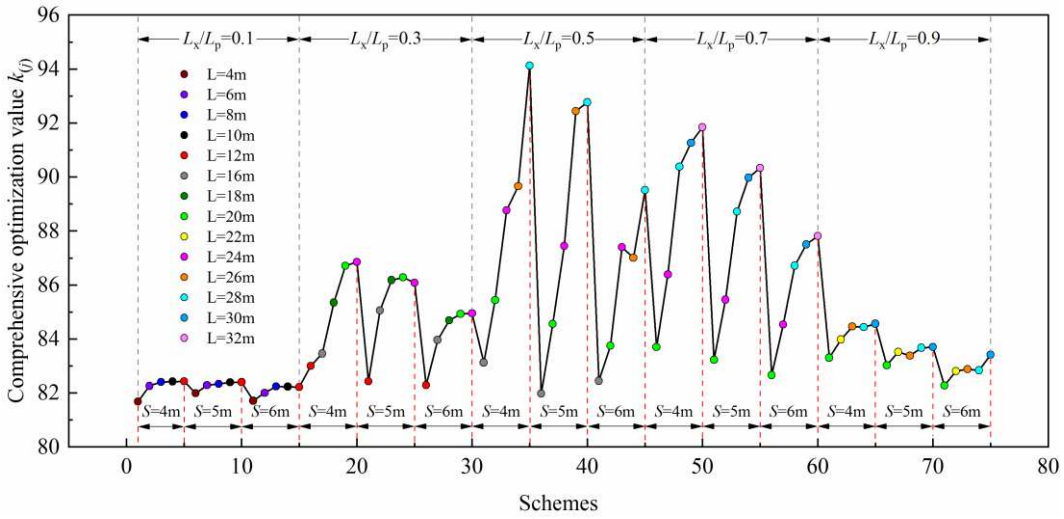

Fig.14 Optimization results based on the multi-objective comprehensive optimization model. S, L_x/L_p stand for the pile spacing and the pile location, respectively. For interpretation of the references to color in this figure, the reader is referred to the electronic version of this page.

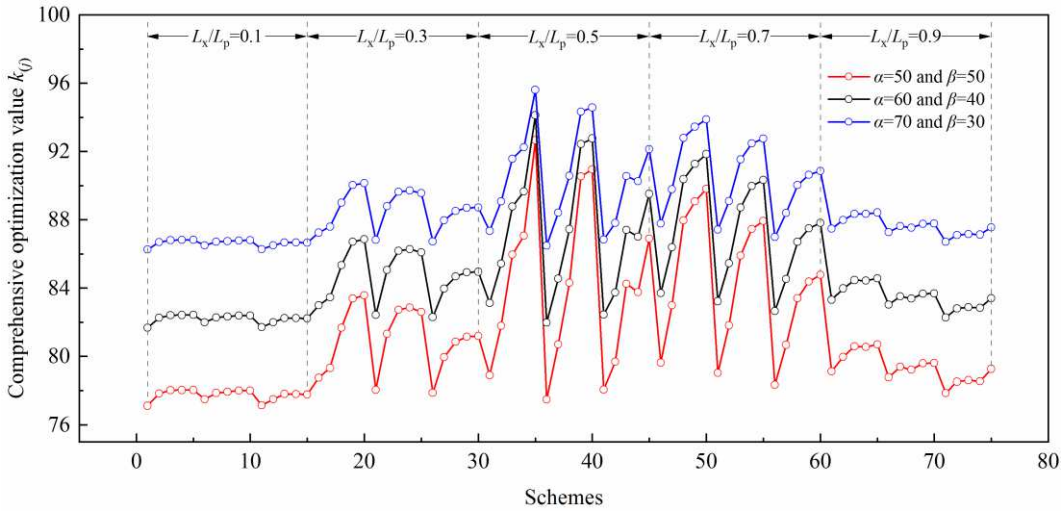

852

853

854 **Fig.15** Comparison of optimization results with different α and β values (Refer to Tables 3-7 or Fig.

855 14 for detailed reinforcement scheme corresponding to scheme number). For interpretation of the

856 references to color in this figure, the reader is referred to the electronic version of this page.

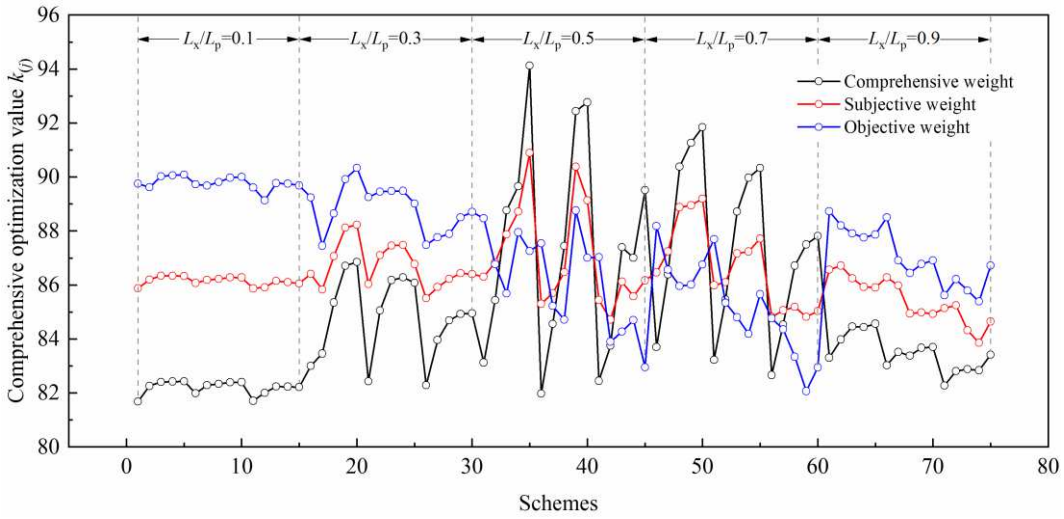

Fig.16 Comparison of optimization results with different weights (Refer to Tables 3-7 or Fig. 14 for detailed reinforcement scheme corresponding to scheme number). For interpretation of the references to color in this figure, the reader is referred to the electronic version of this page.